PARTICLE ROLLING AND ITS EFFECTS IN GRANULAR MATERIALS

Matthew R. Kuhn,
Dept. of Civ. and Env. Engrg., School of Engrg.,
Univ. of Portland, 5000 N. Willamette Blvd., Portland, OR 97203, USA,
Tel. 503-943-7361, Fax 503-943-7316, kuhn@up.edu.

Katalin Bagi,
Hungarian Academy of Sciences, Research Group for Computational Structural Mechanics,
Technical University of Budapest, Budapest H–1521, Hungary, kbagi@mail.bme.hu.

ABSTRACT

The paper includes a summary of previous work, currently in review, concerning alternative definitions of the relative rotation and rolling between particle pairs. These definitions provide a basis for objective contact mechanisms that include the effects of relative rotational movements as well as the relative translations of the particles at a contact. The definitions of rolling can also be used to decompose the motions of two particles into separate modes: sliding, rolling, and rigid-body motions of the pair. The rolling mode is investigated in 2D and 3D numerical simulations, in which we measure the intensity of contact rolling as the entire assembly is deformed. We also consider the spatial distribution of rolling in a 2D numerical simulation, for which the local movements and deformations are more easily visualized.

1. INTRODUCTION

Granular materials are large assemblies of particles that interact at the contacts of particle pairs. The particle interactions can take numerous forms, all of which contribute to a material's bulk stress and deformation characteristics. As an example, early studies showed that stress is borne in an uneven manner during the deviatoric loading of a granular material: "force chains" of heavily loaded particles support most of the deviatoric stress when a granular material is loaded from an initially isotropic state. This redistribution and evolution in force transmission is due to one form of the motions among particle pairs, in particular, those motions that produce a deformation of the grains at their contacts. Another form of particle motions was recognized by Oda and his co-workers in their early experiments on model assemblies of oval shape disks [1]. They found that particle rotations become quite large at even modest deviatoric strains, and they identified particle rolling as a dominant characteristic of the deformation of granular materials. They also speculated that rolling produced a softening effect, and that particle rolling would partially negate the strengthening effect of inter-granular friction. This assumption coincides with the view of Thornton [2] who considered contact friction as a kinematic constraint that gives rise to particle rolling. Several forms of rotational patterning have been identified by the authors, who have employed various visualization techniques to explore the results of computer

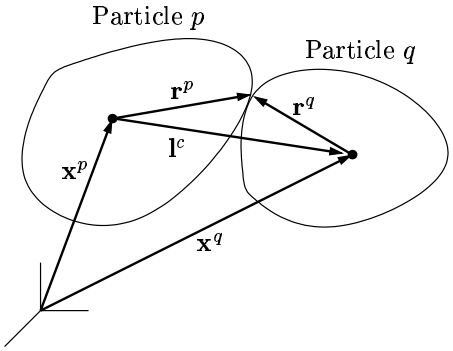

Figure 1. Two particles in contact.

(DEM) simulations of biaxial compression in two-dimensional (2D) assemblies [3]. These patterns included the formation of thin bands of particles that trend in directions oblique to the principal deformation axes, and within these bands the particles rotate in a common direction.

The authors embarked upon a program to scrutinize the rotational and rolling motions that occur during the deformation of a granular material. To do so, we first had to develop a vocabulary and definitions for the various forms of inter-particle movements. These forms are presented in Section 2 and include deformation, rolling, twisting, and rigid rotation modes. Even the simple term "rolling" admits numerous definitions, and the choice of one or another definition depends as much upon perception and preference, as it does upon the contact mechanics. We were guided, in part, by the studies of Iwashita and Oda [4], who defined a type of rolling between 2D circular disks, and this and other definitions are extended to 3D particles of arbitrary shape. In Section 3 we present the results of simple DEM simulations of biaxial and triaxial loading. Various features of the rolling motion are discussed.

2. DEFINITIONS OF ROLLING

Consider two particles, p and q, to which we assign the material reference points $\boldsymbol{\chi}^p$ and $\boldsymbol{\chi}^q$ (Fig. 1). These reference points are located at positions $\mathbf{x}^p$ and $\mathbf{x}^q$ relative to the global axes. The two particles are in contact, and the vectors $\mathbf{r}^p$ and $\mathbf{r}^q$ connect the reference points $\boldsymbol{\chi}^p$ and $\boldsymbol{\chi}^q$ to the contact point; whereas the branch vector $\mathbf{l}$ connects the two reference points: $\mathbf{l} = \mathbf{r}^p - \mathbf{r}^q$. The contact is assumed to be point-like—the contact area is negligibly small in comparison with the displacements. The particles undergo the incremental translational and rotational movements $d\mathbf{u}^p$, $d\mathbf{u}^p$, $d\boldsymbol{\theta}^p$, and $d\boldsymbol{\theta}^q$ during the time increment dt. These four movement vectors are described by twelve scalar components, which form a 12-dimensional vector space of possible movements. In classical kinematics, the particles might be truly rigid, and, hence, prevented from inter-penetration (a non-holonomic constraint), but the behavior of granular materials is influenced by the local particle deformations at their contacts. These deformations are produced by the relative motions of the two particles,

$$d\mathbf{u}^{\text{def}} = (d\mathbf{u}^q - d\mathbf{u}^p) + (d\boldsymbol{\theta}^q \times \mathbf{r}^q - d\boldsymbol{\theta}^p \times \mathbf{r}^p) \ , \tag{1}$$

which can be separated into components that are tangent and normal to the contact surface [5, 6, 7]. The deformation motion (1) accounts for three of the twelve degrees of freedom of the particle pair. The deformation motion is objective, since its scalar components would be properly reported by two observers having independent motions [8]. Because the contact deformation is objective, it may be used in a constitutive description of the contact force–deformation relationship.

The authors have identified three definitions of rolling motion. The simplest is based on the relative rotation of the particle pair,

$$d\boldsymbol{\theta}^{\text{rel}} = d\boldsymbol{\theta}^{q} - d\boldsymbol{\theta}^{p} \ , \tag{2}$$

and, like the deformation motion in (1), the relative rotation (2) is clearly objective. The motion $d\boldsymbol{\theta}^{\text{rel}}$ can be separated into two components, one aligned with and the other orthogonal to the contact normal $\mathbf{n}$:

$$d\boldsymbol{\theta}^{\text{rel, roll, 1}} = d\boldsymbol{\theta}^{\text{rel}} - (d\boldsymbol{\theta}^{\text{rel}} \cdot \mathbf{n})\mathbf{n} \tag{3}$$

$$d\boldsymbol{\theta}^{\text{rel, twist}} = (d\boldsymbol{\theta}^{\text{rel}} \cdot \mathbf{n})\mathbf{n} \ , \tag{4}$$

where the contact normal $\mathbf{n}$ is directed outward from particle p. The index "1" denotes the name "Type 1" rolling, as described by the authors [9]. The four motions (1)–(4) would be assigned opposite (negative) values if the indices p and q are exchanged. When plotting graphic visualizations of simulation results, we have often used alternative forms of (3) and (4), since the values of these forms do not depend upon the order of the indices:

$$d\boldsymbol{\theta}^{\text{rel, roll, 1}} \times \mathbf{n} \tag{5}$$

$$d\boldsymbol{\theta}^{\text{rel, twist}} \cdot \mathbf{n} \ . \tag{6}$$

A second form of rolling is based upon a particular average of the motions of two material points, one attached to each of the particles at their contact, like the teeth of two inter-meshed gears moving in unison. The average translational velocity of the two points (e.g. the opposing gear teeth) is, of course, not objective, and the magnitude of its tangential-direction component $du^{\mathbf{t}\text{-avr}}$,

$$du^{\mathbf{t}\text{-avr}} = \frac{1}{2}\left[(d\mathbf{u}^{p} + d\boldsymbol{\theta}^{p} \times \mathbf{r}^{p}) \cdot \mathbf{t} + (d\mathbf{u}^{q} + d\boldsymbol{\theta}^{q} \times \mathbf{r}^{q}) \cdot \mathbf{t}\right] \ , \tag{7}$$

is also not objective. However, the motions that are associated with the common rigid-body-like rotation of the pair can be subtracted from $du^{\mathbf{t}\text{-avr}}$ to produce an objective measure of rolling [7]:

$$du^{\mathbf{t}\text{-roll, 2}} = \frac{1}{2}\left[(d\boldsymbol{\theta}^{p} \cdot \mathbf{z}^{t})(\mathbf{r}^{p} \cdot \boldsymbol{\lambda}^{t}) + (d\boldsymbol{\theta}^{q} \cdot \mathbf{z}^{t})(\mathbf{r}^{q} \cdot d\boldsymbol{\lambda}^{t}) - \frac{(d\mathbf{u}^{q} - d\mathbf{u}^{p}) \cdot \mathbf{t}}{\ell^{\perp t}}(\mathbf{r}^{p} + \mathbf{r}^{q}) \cdot \boldsymbol{\lambda}^{t}\right] \ , \tag{8}$$

where the unit vectors $\mathbf{z}^{t}$ and $\boldsymbol{\lambda}^{t}$ depend upon the directions of a tangent vector $\mathbf{t}$ and the branch vector $\mathbf{l}$:

$$\boldsymbol{\lambda}^{t} = \mathbf{l}^{\perp t}/\ell^{\perp t} \ , \quad \mathbf{z}^{t} = \boldsymbol{\lambda}^{t} \times \mathbf{t} \ , \tag{9}$$

with

$$\mathbf{l}^{\perp t} = \mathbf{l} - (\mathbf{l} \cdot \mathbf{t})\mathbf{t}, \quad \ell^{\perp t} = |\mathbf{l}^{\perp t}| \ . \tag{10}$$

The quantity $du^{\mathbf{t}\text{-roll, 2}}$ is termed "Type 2" rolling. Similar measures of rolling that are associated with the normal $\mathbf{n}$ or another tangent direction (say, direction $\mathbf{w}$) can be computed by substituting $\mathbf{n}$ or $\mathbf{w}$ in equations (8)–(10).

A third form of rolling is based upon the paths of the contact points as they travel across the two surfaces while the particles move. For example, when two inter-meshed gears rotate, the contact point moves from tooth to tooth around the two gears. This form of rolling requires a knowledge of the local surface curvatures of the two particles at the contact [10, 8]:

$$d\mathbf{u}^{\text{roll, 3}} = -(\mathbf{K}^{p} + \mathbf{K}^{q})^{-1}\left[d\boldsymbol{\theta}^{\text{rel}} \times \mathbf{n} + \frac{1}{2}(\mathbf{K}^{p} - \mathbf{K}^{q})\, d\overline{\mathbf{u}}^{\text{def}}\right] \ , \tag{11}$$

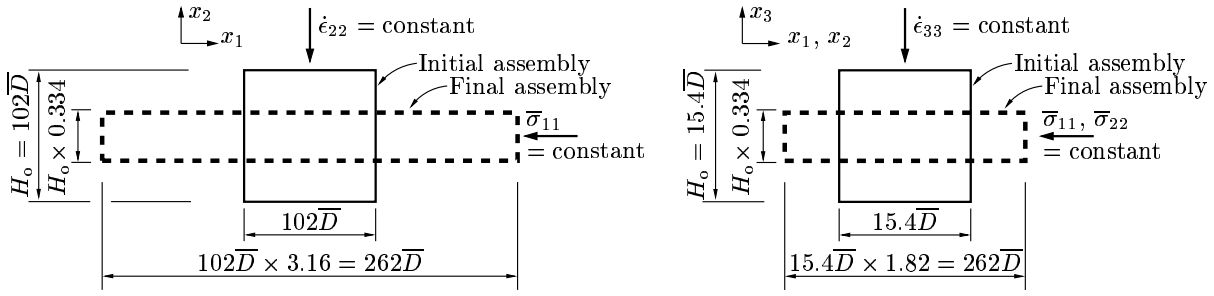

(a) 2D assembly (b) 3D assembly

Figure 2. Biaxial and triaxial loading conditions for the simulated compression of a disk and sphere assemblies. The initial and final sizes are shown to scale. All boundaries are periodic. The disk assembly was initially square; the sphere assembly was initially a cube.

where $\mathbf{K}^p$ and $\mathbf{K}^q$ are the surface curvature tensors, and $d\overline{\mathbf{u}}^{\text{def}}$ is the component of $d\mathbf{u}^{\text{def}}$, defined by (1), in the tangent plane of the contact. This "Type 3" rolling is clearly objective, since it is a linear combination of the objective motions $d\mathbf{u}^{\text{def}}$ and $d\boldsymbol{\theta}^{\text{rel}}$. The vector $d\mathbf{u}^{\text{roll, 3}}$ lies in the tangent plane of the contact, and its value is independent of the order of particles p and q. Because it always lies in the tangent plane, $d\mathbf{u}^{\text{roll, 3}}$ is restricted to a 2-dimensional subspace of vectors. The rolling translation $d\mathbf{u}^{\text{roll, 3}}$ should, therefore, be supplemented with an auxiliary rolling quantity, say $d\boldsymbol{\theta}^{\text{rel, twist}}$, to complete the 6-dimensional subspace of objective motions (for example, a subspace formed from the motions $d\mathbf{u}^{\text{def}}$, $d\mathbf{u}^{\text{roll, 3}}$, and $d\boldsymbol{\theta}^{\text{rel, twist}}$). Motions that lie outside of this six-dimensional space, but within the 12-dimensional space of all motions, are non-objective [9].

3. SIMULATION EXAMPLE

The rates and influence of contact rolling were measured in numerical simulations of biaxial and triaxial compression. A conventional implementation of the Discrete Element Method (DEM) was used to simulate the quasi-static behavior of large 2D and 3D assemblies of 10,816 unbonded circular disks and 4096 spheres. The disk and sphere sizes were randomly distributed over a fairly narrow range of between 0.56–$1.7\overline{D}$ (disks) and 0.49–$1.35\overline{D}$ (spheres), where $\overline{D}$ is the mean particle diameter. The material was created by slowly and isotropically compacting a sparse arrangement of particles, during which friction between particle pairs was disallowed (friction was later restored for the compression tests). This compaction technique produced a material that was dense, random, and isotropic, at least when viewed at a macro-scale. The square and cube assemblies were surrounded by periodic boundaries, a choice that eliminates any non-uniformities that might otherwise occur in the vicinity of rigid platens or assembly corners.

A single loading test was conducted on each of the two assemblies. The height of each assembly was reduced at a constant rate of compressive strain until its final height was less than half of the original height, while maintaining a constant average horizontal stress along the side boundaries, as in Figure 2. The large strains were sufficient to eventually attain a steady state (critical state) condition in which the stress and volume remained constant, even as deformation proceeded. Over 10×10^6 numerical time steps were required to reach the final vertical (engineering) strain, $\overline{\varepsilon}_{22} = -0.59$, and at this rate of loading, the average imbalance of force on a particle was typically less than $4{\times}10^{-4}$ times the average contact force.

During compression loading, a simple force mechanism was employed between contacting particles. The particles were unbonded, so that no inter-particle tensile forces could develop.

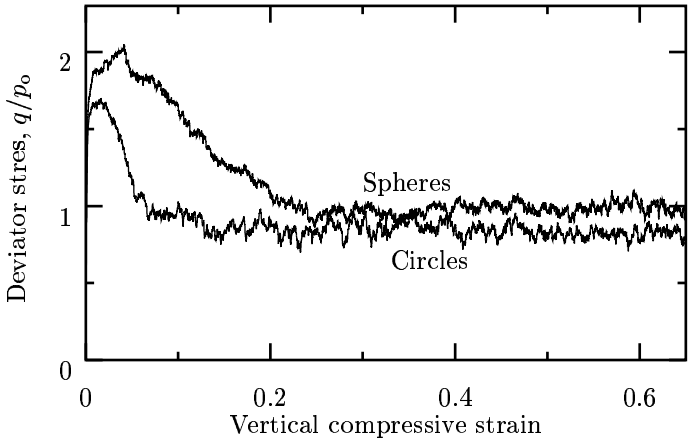

Figure 3. Loading of 2D and 3D assemblies of circular disks and spheres. The deviator stress is shown in a dimensionless form by dividing by the initial pressure p_o.

Table 1. Conditions at three strains for the biaxial compression of 10,200 circular disks.

	State		
	Zero strain	Peak state	Steady state
Vertical strain	0	0.003	0.549
Number of contacts, M	20640	17460	15960
Number effective particles, $\overline{N}$	10120	9860	9720
Avg. coord. no., $2N/M$	3.82	3.23	2.95
Avg. eff. coord. no., $2M/\overline{N}$	4.08	3.54	3.29
Void ratio, e	0.1727	0.1727	0.2362
a) $\lvert\mathrm{Mean}(d\mathbf{u}^{\mathrm{roll\ 2,3}}/\overline{D}/d\epsilon)\rvert$	0.0013	0.014	0.059
b) $\mathrm{Mean}(\lvert d\mathbf{u}^{\mathrm{roll\ 2,3}}/\overline{D}/d\epsilon\rvert)$	0.26	2.74	14.8
c) $\mathrm{Std}(\lvert d\mathbf{u}^{\mathrm{roll\ 2,3}}/\overline{D}/d\epsilon\rvert)$	0.23	4.08	31.2

All contact forces were short-range—only particles that were touching could develop a repulsive contact force, and this force depended on the numerical overlap between a contacting particle pair. Linear normal and tangential contact springs were assigned equal stiffnesses ($k^{\mathrm{n}} = k^{\mathrm{t}}$), and slipping between particles would occur whenever the contact friction coefficient of 0.50 was attained—an inter-particle friction angle of 26.6°.

3.1. Assembly of circular disks (2D)

We investigated the behavior of the disk assembly at three strains: at the start of loading ("zero strain"), at the condition of peak deviator stress ("peak state"), and at the "steady state" (Fig. 3). The assembly's fabric at these three states is summarized in Table 3.1. The number of contacts is substantially reduced at both the peak and steady states, and the number of *effective* particles, those having two or more contacts, is also reduced. Intense dilation occurs prior to and beyond the peak state, and greatly reduces the average and effective coordination numbers.

We will focus on the rolling of Types 2 and 3 of Eqs. (8) and (11), which, for circular particles, are equal and occur entirely in the tangent direction (because of the particular manner in which they were defined, however, the two types of rolling occur in opposite directions). A summary of Types 2 and 3 rolling in the disk assembly is given in the lower half of Table 3.1, which reports the mean rolling rate and its statistical dispersion among the 9,700 to 10,100 contacts within the 2D assembly. We have expressed the rolling translations $d\mathbf{u}^{\mathrm{roll}}$ in a dimensionless form by dividing by the vertical strain increment $d\epsilon$ and by the mean particle

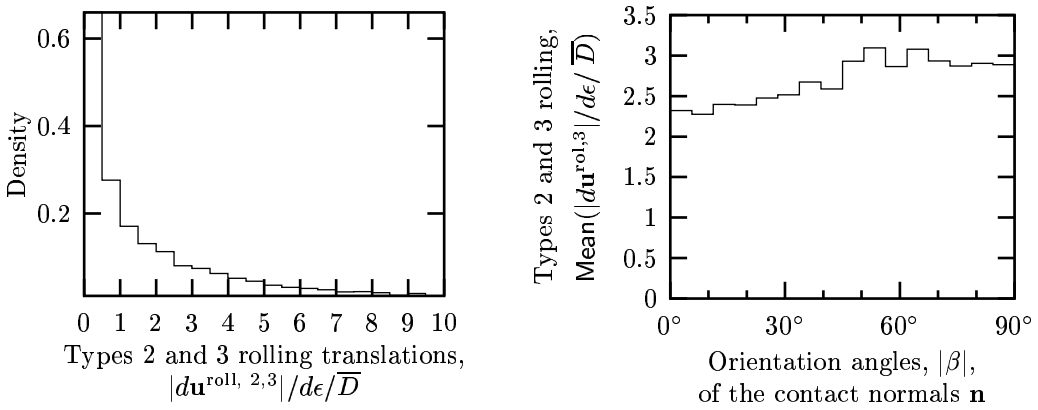

(a) Distribution of rolling rates

(b) Polar distribution of the mean rolling rates

Figure 4. Distribution of Types 2 and 3 rolling during biaxial compression of a disk assembly.

diameter $\overline{D}$. The product $\overline{D}d\epsilon$ is a rough measure of the relative translations among nearby particles during the deformation increment $d\epsilon$. The rolling translations $d\mathbf{u}^{\text{roll}}$ are vectors whose directions are independent of the particular ordering of the particle pairs (i.e., independent of an exchange of indices p and q, as in Section 2). To extract meaningful averages from this set of vectors, we report the magnitude of the mean of the vectors (row a, Table 3.1) and the mean and standard deviation of their magnitudes (rows b and c). The mean of the rolling vectors is quite small (row a) at all three strains, which suggests that there is no preferred direction of rolling, as might be the case within a dominant shear band. The mean *magnitude* of rolling at zero strain (row b) is also small: a value of 0.23 indicates that the rolling occurs at rates much smaller that the average relative motions of nearby particle pairs. The rolling rate at the peak state, however, is very large, and the steady state, the rolling rates are extreme. A histogram of the distribution of rolling rates at the peak state is given in Fig. 4a, which shows that many contacts (about 17% of all contacts) are rolling at rates greater than 5 times $\overline{D}d\epsilon$. Large rolling rates are also pervasive throughout the assembly at the peak state, and fewer than 33% of the contacts have rolling rates less than $0.5\overline{D}d\epsilon$. At all strains, rolling occurs among contacts of all orientations, as is shown in Fig. 4b. In this figure, the orientation of the contact normal $\mathbf{n}$ is an angle β measured from the horizontal axis: $\beta = \arccos(\mathbf{n} \cdot \mathbf{e}_2)$.

Although we have not yet analyzed all of the data, we have observed one unusual spatial pattern in the rolling among circular disks. Figure 5 shows a small subset of the assembly, a representative subset of fewer than 450 particles. The arrows indicate the rolling vectors $d\mathbf{u}^{\text{roll}}$ for each contact at the peak state (some contacts have such small rolling rates that their rolling vectors may not be visible). This small sample shows that the largest rolling rates are usually found around a few particles, rather than being more evenly dispersed among all contacts. With each of the most active particles, the rolling vectors are usually directed in a common manner around the particle—the rolling vectors around an active particle are usually either entirely clockwise or entirely counter-clockwise.

3.2. Assembly of spheres (3D)

The 3D assembly of spheres exhibited many of the same characteristics as the 2D assembly of disks. Fabric conditions at zero strain, at the peak state, and at the steady state are given in Table 3.2. As with the assembly of disks, the number of contacts is greatly reduced at the peak state, but only a small reduction occurs between the peak and steady states.

The rolling rates are also shown in Table 3.2, which gives the Type 2 and 3 translational

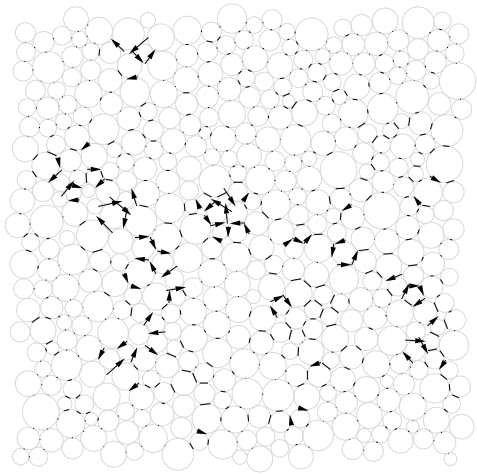

Figure 5. Rolling within a sub-region of the disk assembly.

Table 2. Conditions at three strains for the triaxial compression of 4,096 spheres.

	State		
	Zero strain	Peak state	Steady state
Vertical strain	0	0.003	0.549
Number of contacts, M	11410	8330	8210
Number effective particles, $\bar{N}$	3700	3550	3660
Avg. coord. no., $2N/M$	5.57	4.06	4.01
Avg. eff. coord. no., $2M/\bar{N}$	6.17	4.69	4.49
Void ratio, e	0.509	0.515	0.693
a) $\lvert\text{Mean}(d\mathbf{u}^{\text{roll }2,3}/\overline{D}/d\epsilon)\rvert$	0.0009	0.066	0.051
b) $\text{Mean}(\lvert d\mathbf{u}^{\text{roll }2,3}/\overline{D}/d\epsilon\rvert)$	0.24	5.05	11.2
c) $\text{Std}(\lvert d\mathbf{u}^{\text{roll }2,3}/\overline{D}/d\epsilon\rvert)$	0.15	7.08	10.1
d) $\lvert\text{Mean}(d\boldsymbol{\theta}^{\text{rel, twist}}\cdot\mathbf{n}/d\epsilon)\rvert$	0.006	0.214	0.147
e) $\text{Mean}(\lvert d\boldsymbol{\theta}^{\text{rel, twist}}\cdot\mathbf{n}/d\epsilon\rvert)$	0.56	12.2	27.5
f) $\text{Std}(\lvert d\boldsymbol{\theta}^{\text{rel, twist}}\cdot\mathbf{n}/d\epsilon\rvert)$	0.50	22.4	31.7
g) $\lvert\text{Mean}(d\boldsymbol{\theta}^{\text{rel, roll, 1}}\times\mathbf{n}/\overline{D}/d\epsilon)\rvert$	0.003	0.300	0.319
h) $\text{Mean}(\lvert d\boldsymbol{\theta}^{\text{rel, roll, 1}}\times\mathbf{n}/\overline{D}/d\epsilon\rvert)$	0.98	20.8	46.2
i) $\text{Std}(\lvert d\boldsymbol{\theta}^{\text{rel, roll, 1}}\times\mathbf{n}/\overline{D}/d\epsilon\rvert)$	0.67	31.6	44.3

rates $d\mathbf{u}^{\text{roll}}$ that occur in the tangent planes of the contacts, as well as the twisting rotations $d\theta^{\text{rel, twist}}$ that occur about the contact normals (Eq. 4). The mean vector values of rolling and twisting are small at all strains (rows a and d), suggesting that there is no preferred directions of rolling or twisting. The mean rolling and twisting magnitudes (rows b and e) are modest at zero strain, large at the peak stress, and extreme at the steady state. In these simulations, no spring or other restraint was employed to inhibit twisting at the contacts, and the results show that this form of motion is quite large. It is difficult to compare a translational rate, such as $d\mathbf{u}^{\text{roll}}$, with a rotational rate, such as $d\theta^{\text{rel, twist}}$, but a comparison of the twisting and rolling rotations (rows d–f and g–i) indicate that rolling may be the dominant form of inter-particle motion, although twisting is also significant.

4. CONCLUSION

We have summarized three definitions of rolling, and have conducted numerical simulations to measure their extent during the loading of disk and sphere assemblies. The rolling motions are very large, particularly at large strains, and rolling appears to spatially isolated and patterned. Further studies are ongoing, including the simulation of assemblies of non-circular 2D particles and non-spherical 3D particles, and the results of these studies will be presented at the conference.

REFERENCES

[1] M. Oda, K. Iwashita, and T. Kakiuchi. Importance of particle rotation in the mechanics of granular materials. In R. P. Behringer and J. T. Jenkins, editors, *Powders & Grains 97*, pages 207–210. A. A. Balkema, Roterdam, Netherlands, 1997.

[2] C. Thornton. Force transmission in granular media. *KONA Powder and Particle*, 15:81–90, 1997.

[3] M. R. Kuhn and K. Bagi. Particle rotations in granular materials. In A. W. Smyth, editor, *Proc. 15th ASCE Engineering Mechanics Conf.*, pages 1–7. ASCE, Reston, Va., U.S.A., 2002. on compact disk media and http://www.civil.columbia.edu/em2002/.

[4] K. Iwashita and M. Oda. Rolling resistance at contacts in simulation of shear band development by DEM. *J. Engrg. Mech.*, 124(3):285–292, Mar. 1998.

[5] M. A. Koenders. The incremental stiffness of an assembly of particles. *Acta Mechanica*, 70:31–49, 1987.

[6] C. S. Chang and A. Misra. Computer simulation and modelling of mechanical properties of particulates. *Computers and Geotechnics*, 7(4):269–287, 1989.

[7] K. Bagi and M. R. Kuhn. A definition of particle rolling in a granular assembly in terms of particle translations and rotations. *J. Appl. Mech.*, 2003. In review.

[8] M. R. Kuhn and K. Bagi. An alternative definition of particle rolling in a granular assembly. *J. Engrg. Mech.*, 2003. In review.

[9] M. R. Kuhn and K. Bagi. On the relative motions of two rigid bodies at a compliant contact: application to granular assemblies. 2003. In review.

[10] D. J. Montana. The kinematics of contact and grasp. *Int. J. Robotics Res.*, 7(3):17–32, 1988.